Bendola Publishing
Journal of Transition Metal Complexes
Vol. 3 (2020), Article ID 246100, 15 pages
doi:10.32371/jtmc/246100

Research Article

Synthesis, Characterization and Biological Studies of Cu^{2+}, Ni^{2+}, Cd^{2+}, and Pt^{4+} Complexes Derived from 3-(3H-1,2,4-Triazole-4-(5H)-Ylimino)Butane-2-One-Oxime (L)

Doaa E. El-Kholy and Mohsen M. Mostafa

Chemistry Department, Faculty of Science, Mansoura University, Egypt
Address correspondence to Mohsen M. Mostafa, amohsenmostafa@yahoo.com

Received 22 April 2020; Revised 22 May 2020; Accepted 26 May 2020

Abstract Novel Cu^{2+}, Ni^{2+}, Cd^{2+}, and Pt^{4+} complexes derived from 3-(3H-1,2,4-triazole-4-(5H)-ylimino)butane-2-one-oxime (L) were synthesized and characterized. FTIR spectra propose that L acts in different methods (bi- tri- and/or tetradentate) depending on the metal used. Electronic spectra and magnetic measurements of the complexes suggest a structure that is tetrahedral for Ni^{2+}, octahedral for Cd^{2+}, while square-planar for Cu^{2+} and Pt^{4+} complexes. Density functional theory (DFT) parameters were applied for Cu^{2+}, Ni^{2+}, and Pt^{4+} complexes which prove the geometry of L towards the metal ions. Coats-Redfern and Horowitz-Metzger methods were used to calculate the kinetic and thermodynamic parameters of the isolated complexes. The cyclic-voltammogram curve of the Cu^{2+} complex was reported. The biological activity of L and its complexes were tested against three types of cancer cell lines, and against different bacterial strains.

Keywords complexes of triazole derivatives; biological activity; electronic and magnetic studies

1. Introduction

1,2,4-Triazoles synthesized from the substitution reaction of N-atom of hydrazides or amide N-atom reaction are regarded as an example of cyclic-hydrazides. Recently, 1,2,4-triazoles acquired great importance as a ligand system attributed to the ability to behave as a mono, bi- or tridentate ligand. Noncovalent interactions such as dipole-dipole, hydrogen bonding lone-pair (N)-π, and π-stacking admit numerous varieties of 1,2,4-triazole with biological goals [1,2]. The chemical importance of 1,2,4-triazole system is mainly due to its ability to bridge between different metal centers [3]. Biological activities such as anathematic [4,5], antiviral [6], antifungal [7], antimicrobial [8], hypnotic [9], pesticide [10, 11], mastectomy cancer preventive [12,13], anticancer, anticonvulsant and anti-inflammatory [14,15,16,17,18,19, 20,21,22,23], CNS depressant [24], antitumor [25], and antihypertensive activities are reported for 1,2,4-triazoles [26]. $[Cu_3LCl_2(H_2O)_5]4Cl$, $[NiLCl(H_2O)]Cl \cdot 1.5H_2O$, $[Pt_2LCl_5(EtOH)_{0.5}(H_2O)_{0.5}]3Cl$, and $[Cd_3LCl_6(H_2O)_7]$ were obtained and characterized. All the complexes were distinctive by different tools including chemical (C, H, M, Cl), spectral (IR, UV-Vis), TGA, and magnetic moments. The biological activity of the ligand 3-(3H-1,2,4-triazole-4-(5H)-ylimino)butane-2-one-oxime (L) and its complexes was tested.

2. Experimental

2.1. Materials and methods

The solvents and chemicals used herein were of AR quality, such as 2,3-Butanedione-monoxime (BDH; Poole, UK), hydrazine hydrate (Fisher Scientific; MA, USA), ethyl formate (Merck; NJ, USA), $NiCl_2 \cdot 6H_2O$, $CuCl_2 \cdot 2H_2O$, $CdCl_2$, and H_2PtCl_6. The chemicals, solvents, and apparatus as well as the methods of analyses were used as reported earlier [27].

2.2. Preparation of L

L, (E)-N-[(3E)-3-[(4H-1,2,4-triazol-4-yl)imino]butan-2-ylidene]hydroxylamine was synthesized as discussed in our earlier work [28].

2.3. Preparation of complexes

2.3.1. Synthesis of Ni^{2+} complex

$[NiLCl(H_2O)]Cl \cdot 1.5H_2O$ was obtained by adding the ligand (0.50 g; 3 mmol) in ethanol to an ethanolic solution of $NiCl_2 \cdot 6H_2O$ (0.72 g; 3 mmol). The green gel mixture at pH = 5.0 was formed and then the reactants were refluxed for 7 h. Finally, the complex was separated from the filtrate, continuously washed with ether, and finally dried in a dryer (yield: 60%). Elemental analyses: Anal. Found: for $C_6H_{14}Cl_2NiN_5O_{2.5}$ (%): C, 21.2; H, 4.2; Ni, 18.1; Cl, 21.5. Calcd.: (%) C, 21.1; H, 4.1; Ni, 17.2; Cl, 20.7, m.p. 233 °C, Λ_m: 47 ohm^{-1} cm^2 mol^{-1} and μ_{eff}: 4.03 BM.

2.3.2. Synthesis of Pt^{4+} complex

$[Pt_2LCl_5(H_2O)_{0.5}(C_2H_5OH)_{0.5}]3Cl$ was formed by adding the ligand (0.33 g; 2 mmol) dissolved in ethanol (15 mL) to a

solution of H_2PtCl_6 (0.82 g; 2 mmol) in EtOH (10 mL). The pH of the mixture was found to be 3–4. Yellow precipitate was formed at once then the reactants were refluxed with stirring on a heater for 6 h. The resulting solid compound was separated by filtration, laved several times by diethyl ether, and then left to dehydrate in a vacuum dryer over P_4O_{10} (yield: 60%). Elemental analyses: Anal. Found: for $C_7H_{13}Cl_8Pt_2N_5O_2$ (%): C, 9.5; H, 1.8; Pt, 45.3; Cl, 31.7. Calcd.: (%) C, 9.6; H, 1.5; Pt, 44.7; Cl, 32.5, m.p. $> 300\,^{\circ}C$, Λ_m: 96 $ohm^{-1}\,cm^2\,mol^{-1}$ and μ_{eff}: diamagnetic.

2.3.3. Synthesis of Cd^{2+} complex

$[Cd_3LCl_6(H_2O)_7]$ was synthesized by adding the ligand (0.33 g; 2 mmol) soluble in ethanol (15 mL) to $CdCl_2 \cdot H_2O$ (0.40 g; 2 mmol) disbanded in EtOH (10 mL). The pH of the solution was found to be 6.0. A white precipitate was obtained and the reactant was refluxed with stirring on a heater for 7 h. The resulting solid product was separated by filtration, laved many times by diethyl ether, and then dried in a dryer over phosphorous pentaoxide (crop: 50%). Elemental analyses: Anal. Found: for $C_6H_{23}Cl_6Cd_3N_5O_8$ (%): C, 8.6; H, 1.9; Cd, 40.1; Cl, 24.9. Calcd.: (%) C, 8.5; H, 2.4; Cd, 40.0; Cl, 25.2, m.p. $> 300\,^{\circ}C$, Λ_m: 12 $ohm^{-1}\,cm^2\,mol^{-1}$ and μ_{eff}: diamagnetic.

2.3.4. Preparation of Cu^{2+} complex

The Cu^{2+} complex with the general formula $[Cu_3LCl_2(H_2O)_5]4Cl$ was synthesized by adding the ligand (0.167 g; 1 mmol) disbanded in 15 mL of EtOH to a solution of $CuCl_2 \cdot 6\,H_2O$ (0.48 g; 2 mmol) dissolved in 10 mL of EtOH. The reaction mixture was adjusted at pH in the range 3–4 and the reactants were then refluxed with stirring for 8 h. Pale green precipitate was formed and its yield equals about 60%. The resulting solid complex was obtained by filtration, washed continuously with diethyl ether, and then left to dry in a dryer over P_4O_{10}. Elemental analyses: Anal. Found: for $C_6H_{19}Cl_6Cu_3N_5O_5$ (%): C, 11.4; H, 2.1; Cu, 29.1; Cl, 32.9. Calcd.: (%) C, 10.9; H, 2.8; Cu, 28.8; Cl, 32.2, m.p. 220 °C, Λ_m: 124 $ohm^{-1}\,cm^2\,mol^{-1}$ and μ_{eff}: 0.98 BM.

2.4. Molecular modeling

Cluster calculations using $DMOL^3$ program were utilized to attain the structures without any symmetry modality in Materials Studio Package which is determined for achieving of large-scale density functional theory (DFT) calculations [29,30,31,32,33,34].

2.5. Biological studies

2.5.1. Cytotoxic activity

In vitro cytotoxicity of L and four complexes (Cu^{2+}, Cd^{2+}, Pt^{4+}, and Ni^{2+}) was applied against three cancer cell lines [prostate cancer (PC-3), breast cancer (MCF-7), and Hela cell lines] brought from a holding corporation for the products and injections (VACSERA) located in Egypt. The doxorubicin as a typical anticancer medication was used. MTT, DMSO, and RPMI-1640 medium were obtained from Sigma Aldrich (MO, USA) while the fetal bovine serum was obtained from GIBCO (UK). Colorimetric assay effects were recorded at 750 nm using a plate reader (EXL 800). The relative cell practically in rate was computed by using the equation (A570 of treated examples/A570 of uncured sample) × 100. The effect on mammary MCF-7 observed with ELISA and the percentage of safety was estimated using the equation [1-(ODT/ODC)] × 100%, where ODT is the average optical density of cells cured with the compounds and ODC is the average optical density of uncured cells [35,36].

2.5.2. Antibacterial and antifungal activity

In order to test the complexes against two classes of bacteria: *Staphylococcus aurous* (Gram-positive) and *Escherichia coli* (Gram-negative), and two kinds of fungi: *Candida albicans* and *Aspergillus flavus*, the disc diffusion method was utilized [37,38].

2.5.3. Antioxidant activity and screening assay for erythrocyte hemolysis

Samples of blood from the rats were withdrawn in heparinized tubes. Red blood cells (RBCs) were detached from plasma and the buffy coat was washed about three times with 10 volumes of 0.15 M saline solution. After the middle of the last launder, the erythrocytes were centrifuged at 2,500 rpm for 10 min to obtain a constantly packed cell preparation. In the measured coordination polymer system, erythrocyte hemolysis was permeated by peroxyl radicals [39,40]. The same volume of 10% suspension of erythrocytes in a phosphate-buffered saline (PBS; pH = 7.4) and 200 mM 2,2′-azobis(2-amidinopropane) dihydrochloride solution were added to each other in PBS containing samples to be examined at varied concentrations. The reactant was cradled gently and incubated at 37 °C for 2 h. After that, the mixture was emptied, diluted with eight volumes of PBS, and centrifuged for 10 min at 1,500 g. The supernatant absorption was recorded at 540 nm. Also, for achieving a complete hemolysis, the reactant was treated with 8 volumes of distilled water, and the supernatant after centrifugation was measured at 540 nm. L-ascorbic acid was wielded as a positive control.

2.5.4. Colorimetric assay for compounds that bind DNA

DNA methyl green (20 mg) was suspended in 100 mL of 0.05 M Tris-HCl buffers (pH 7.5) containing 7.5 mM $MgSO_4$. The mixture was then stirred at 37 °C for one day. Test samples (10 mg, 100 mg, 1,000 mg) were dissolved in EtOH; after that the solvent was separated under vacuum and to each tube 200 μL of the DNA/methyl green solution

Table 1: The most important assignments of the ligand and its complexes.

Compounds	ν(OH) free	ν(OH) (HB)	ν(C=N) oxime	ν(C=N) aliph.	ν(C=N) cyclic	ν(M−N)	ν(M−O)	ν(HOH)
L, $C_6H_9N_5O$	3,216	3,125	1,678	1,658	1,597	—	—	—
$[NiLCl(H_2O)]Cl \cdot 1.5H_2O$	3,421	3,141	1,691	1,626	1,575	422	439	3,326
$[Cd_3LCl_6(H_2O)_7]$	3,322	3,203	1,687	1,661	1,620	424	466	$3{,}429_{(HB)}$ $3{,}281_{(free)}$
$[Pt_2LCl_5(H_2O)_{0.5}(EtOH)_{0.5}]3Cl$	3,313	3,212	1,699	1,621	1,535	434	470	3,517
$[Cu_3LCl_2(H_2O)_5]4Cl$	3,312	3,193	1,687	1,622	1,549	414	448	$3{,}440_{(HB)}$ $3{,}257_{(free)}$

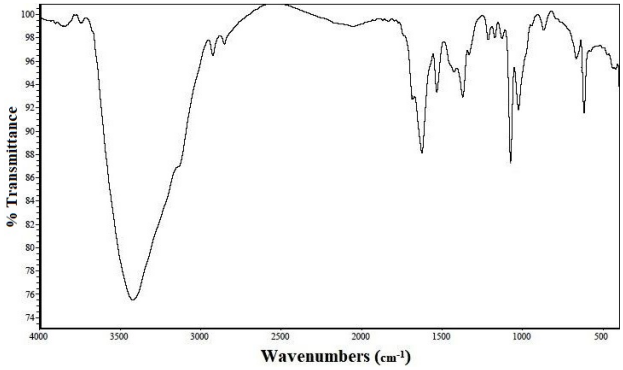

Figure 1: IR spectra of $[NiCl(H_2O)]Cl \cdot 1.5H_2O$.

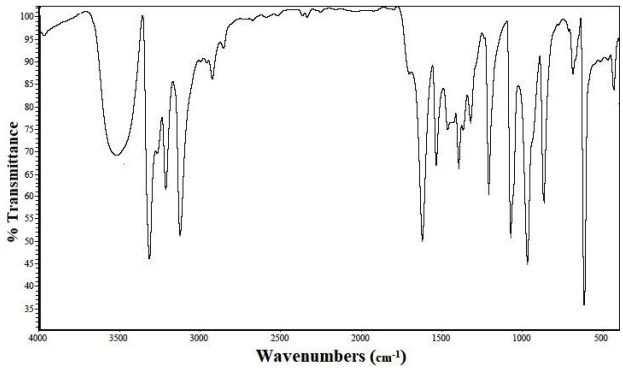

Figure 2: IR spectra of $[Pt_2LCl_5 0.5H_2O 0.5EtOH]$.

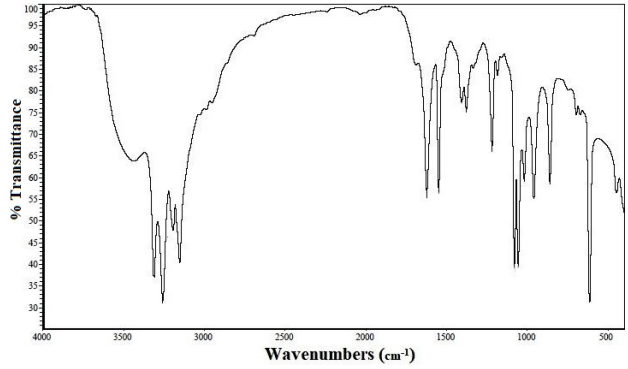

Figure 3: IR spectra of $[Cu_3LCl_2(H_2O)_5]4Cl$.

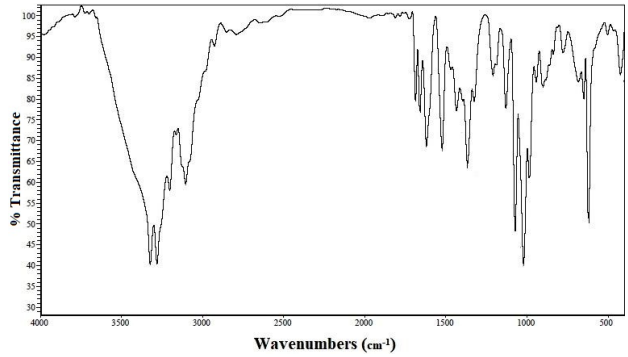

Figure 4: IR spectra of $[Cd_3LCl_6(H_2O)_7]$.

was added. Samples were incubated in the dark at ambient temperature. After one day, the final absorbance of the samples was determined at 642.5–645 nm. Results were corrected for premier absorbance and normalized as the percentage of the untreated standard. The absorbance of the pure DNA ($A_{260/280}$) is ~ 1.8.

3. Results and discussion

3.1. Infrared spectra

The ligand spectrum in KBr exhibits bands at 3,216 sh, 3,125 s, 2,980 m, and 2,784 m cm^{-1} attributed to OH (free), OH (hydrogen-bonded), CH, and CH_3, respectively, as shown in Table 1. Three bands attributed to the azomethine groups: (C=N) at 1,678 cm^{-1}, (C=NOH) at 1,658 cm^{-1}, and (C=N−N) at 1,597 cm^{-1}, are relocated to a lower wavelength in the metal chelates indicating the involvement of these groups in bonding. The IR spectrum of $[NiLCl(H_2O)]Cl \cdot 1.5H_2O$ shows five bands at 3,421 cm^{-1}, 3,141 cm^{-1}, 1,691 cm^{-1}, 1,626 cm^{-1}, and 1,575 cm^{-1} in which the first four bands are directed to low shifts while the latter band is shifted to higher wavenumbers (Figure 1). The first band at 3,421 cm^{-1} refers to the free hydroxyl group of the oxime molecule. Also, the band at 3,141 cm^{-1} refers to the coordinated OH group of H_2O while the two bands at 1,691 cm^{-1} and 1,626 cm^{-1} are assigned to the coordinated

Table 2: The electronic spectra and magnetic moments for L and its complexes.

Compounds	Band position (cm^{-1})	Possible transitions	μ_{eff}
L, $C_6H_9N_5O$	45,871, 41,666	$\pi \rightarrow \pi^*$	—
	38,759	$n \rightarrow \pi^*$	
$[NiLCl(H_2O)]Cl \cdot 1.5H_2O$	20,964	$^3T_1 \rightarrow {}^1T_2$	4.03
	17,605, 14,792	$^3T_1 \rightarrow {}^3T_1(p)$	
	12,903	$^3T_1 \rightarrow {}^3A_2$	
$[Cu_3LCl_2(H_2O)_5]4Cl$	31,645	$n \rightarrow \pi^*$	0.98
	17,543	$d_{z^2} \rightarrow d_{X^2-Y^2}$	
	11,641	$d_{xz}, d_{yz} \rightarrow d_{X^2-Y^2}$	
	10,822	$d_{xy} \rightarrow d_{X^2-Y^2}$	
$[Pt_2LCl_50.5H_2O0.5EtOH]3Cl$	31,446	$n \rightarrow \pi^*$	—
	26,881	$M \rightarrow L$	

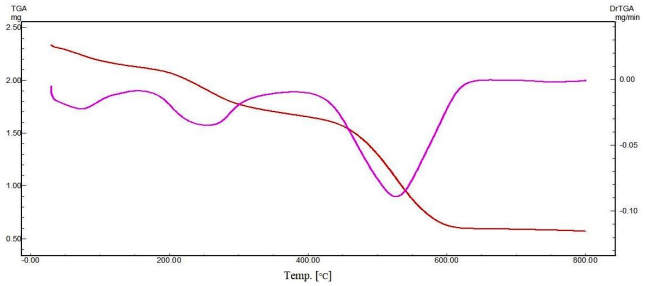

Figure 5: TGA of $[NiLCl(H_2O)Cl]Cl \cdot 1.5H_2O$.

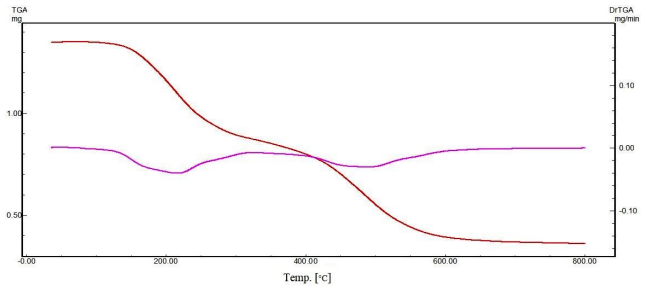

Figure 6: TGA of $[Cu_3LCl_2(H_2O)_5]4Cl$.

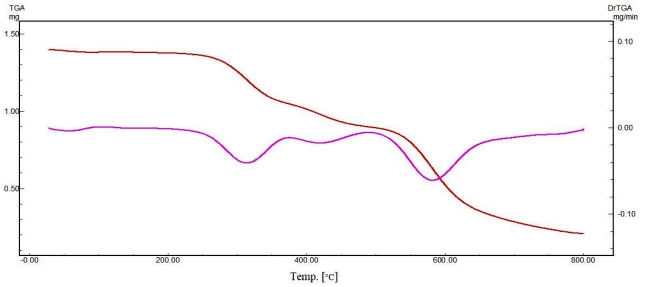

Figure 7: TGA of $[Cd_3LCl_6(H_2O)_7]$.

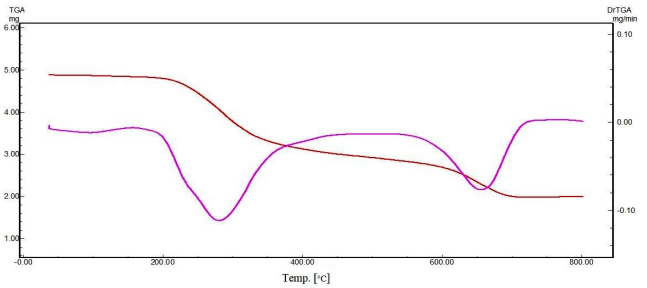

Figure 8: TGA of $[Pt_2LCl_5(H_2O)_{0.5}(EtOH)_{0.5}]3Cl$.

azomethine groups ν [C=$N_{(oxim)}$ and C=$N_{(aliph)}$] vibrations, respectively. Furthermore, the band noticed at 1,575 cm^{-1} refers to the uncoordinated $(C{=}N)_{(cyclic)}$ band [41]. So, the ligand behaves as a tetradentate ligand around the Ni^{2+} ion. The IR spectra of the Cd^{2+}, Pt^{4+}, and Cu^{2+} are recorded in Figures 2–4.

3.2. Electronic spectra and magnetic measurements

The geometries of metal ions in the complexes are assigned according to the positions and number of *d-d* transition peaks that appear in the electronic absorption spectra. The electronic spectra of the ligand and its complexes varied in DMSO. Three bands are observed in the spectrum of L. The first two bands at 45,871 cm^{-1} and 41,666 cm^{-1} are attributed to $\pi \rightarrow \pi^*$ transitions. The third band at 38,759 cm^{-1} is assigned to $n \rightarrow \pi^*$ transition. The visible spectrum of Ni^{2+} complex shows four bands at 20,964 cm^{-1}, 17,605 cm^{-1}, 14,792 cm^{-1}, and 12,903 cm^{-1}; the first band due to $^3T_1 \rightarrow {}^1T_2$ and the second and third bands are assigned to $^3T_1 \rightarrow {}^3T_1(p)$, respectively. The fourth band is assigned to $^3T_1 \rightarrow {}^3A_2$. The magnetic moment of the complex (4.03 BM) suggests a d^8 tetrahedral structure around the nickel ion [42]. Cu complex showed new three bands at 17,543 cm^{-1}, 11,641 cm^{-1}, and 10,822 cm^{-1}, where the first band is assigned $d_{z^2} \rightarrow d_{X^2-Y^2}$ and the other two bands are attributed to $d_{xz}, d_{yz} \rightarrow d_{X^2-Y^2}$ and $d_{xy} \rightarrow d_{X^2-Y^2}$, respectively. The μ_{eff} of the complex (0.98 Bohr Magneton) proposed a d^9 square-planar structure around the Cu^{2+} ion [42]. The two bands (31,446 cm^{-1} and 26,881 cm^{-1}) of the diamagnetic Pt^{4+} complex are assigned

Table 3: The most thermal decomposition steps of the complexes.

Compound	Decomposition steps	Temperature range (°C)	Removed species	Wt. loss	
				% (Found)	% (Calcd.)
$[NiLCl(H_2O)]Cl \cdot 1.5H_2O$	1st	30–120	$1.5H_2O$	8.42	7.91
	2nd	120–466	H_2O+Cl_2	26.21	26.01
	3rd	466–800	$C_4H_9N_5O$	41.94	41.87
	Residue	800	Ni+2C	24.43	24.19
$[Cu_3LCl_2(H_2O)_5]4Cl$	1st	36–328	$5H_2O$+4HCl	36.34	35.71
	2nd	328–524	$C_3H_5N_5OCl_2$	29.79	29.97
	Residue	524–800	3CuC	33.87	34.31
$[Cd_3LCl_6(H_2O)_7]$	1st	28–396	$7H_2O$+3HCl	27.31	27.93
	2nd	396–756	$C_6H_6N_5OCl_3$	33.01	32.08
	Residue	756–800	3Cd	39.68	39.99
$[Pt_2LCl_5(H_2O)_{0.5}(EtOH)_{0.5}]3Cl$	1st	37–306	$0.5(H_2O$+EtOH)+HCl+$2Cl_2$	24.21	24.09
	2nd	306–598	$C_3N_4OCl_2$	20.36	20.5
	3rd	598–670	C_3H_8NCl	10.66	10.71
	Residue	670–800	2Pt	44.77	44.69

Table 4: Kinetic parameters of Cu^{2+}, Ni^{2+}, and Pt^{4+} complexes evaluated by Horowitz-Metzger (HM) and Coats-Redfern (CR) methods.

Step	Mid (Temp (K))	Method	Ea (KJ/mol)	A (S^{-1})	ΔH* (KJ/mol)	ΔS* (KJ/mol)	ΔG* (KJ/mol)
				Ni^{2+} complex			
1st	80	CR	36.9	2×10^4	34.03	−0.18	96.3
		HM	42.61	1×10^6	39.68	−0.28	96.91
2nd	295	CR	83.06	1.87×10^6	78.44	−0.13	150.8
		HM	91.78	0.86×10^9	87.38	−0.28	150.78
3rd	633	CR	142.92	0.9×10^7	137.58	−0.1	216.16
		HM	156.93	0.41×10^{11}	150.01	−0.29	216.67
				Pt^{4+} complex			
1st	170	CR	109.56	1.58×10^9	106.69	−0.07	130.9
		HM	118.25	1.16×10^7	113.97	−0.28	130.11
2nd	450	CR	73.09	0.54×10^4	68.47	−0.13	167.89
		HM	83.38	0.06×10^6	78.05	−0.28	167.18
3rd	635	CR	387.47	1.35×10^{20}	381.93	0.13	292.87
		HM	399.57	0.58×10^{17}	392.01	−0.3	292.27
				Cu^{2+} complex			
1st	444	CR	117.17	4.32×10^{11}	113.47	−0.025	124.79
		HM	125.06	3.83×10^{12}	121.37	−0.007	124.63
2nd	710	CR	88.73	1.03×10^4	82.82	−0.175	207.4
		HM	101.61	1.02×10^5	95.72	−0.156	206.43

to $n \rightarrow \pi^*$ and $M \rightarrow L$ transitions, respectively, and the results are recorded in Table 2.

3.3. Thermal analysis

The analysis of TGA plays an important role in studying the attributes of the metal complexes. The curves are consummated to make sure that the suggested formulae and the structures of the complexes under investigation are correct. A thermo-gravimetric analysis was performed in the range from 20 °C up to 800 °C. TGA results were utilized to appraise and calculate mass loss in addition to the results of the elemental analyses. The decomposition steps for $[NiLCl(H_2O)]Cl \cdot 1.5H_2O$ are depicted in Figure 5. The first started from 30 °C to 120 °C gets along with the loss of one and half H_2O molecules (Found: 8.4%, Calcd.: 7.9%). The second and third steps show losses in the 120 °C to 800 °C corresponding to the removal of H_2O molecule and the fragments of $C_4H_9N_5OCl_2$ (Found: 68.2%, Calcd.: 67.8%). The residue corresponds to Ni+2C in the theoretical loss (24.1%), which is matching the experimental loss 23.4%. The TGA curves for the Ni^{2+}, Cu^{2+}, Cd^{2+}, and Pt^{4+} complexes are shown in Figures 5–8. The results of thermal

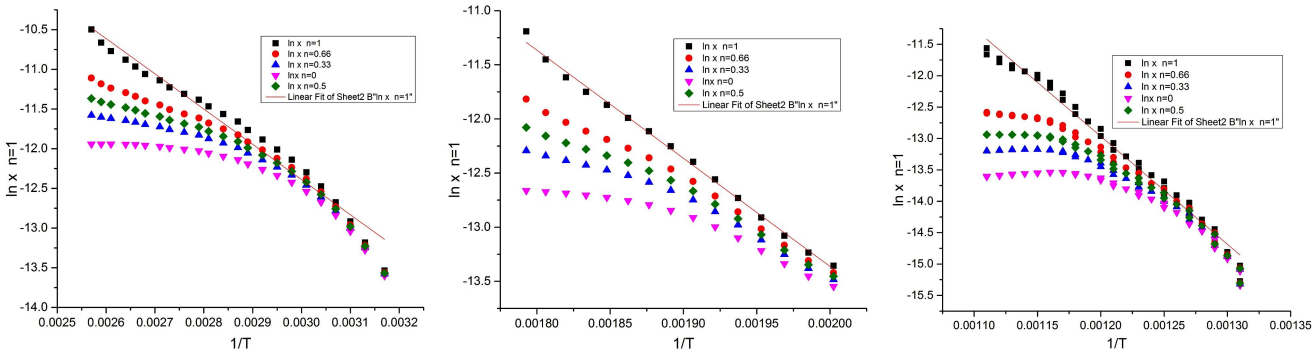

(a) (b) (c)

Figure 9: 1st, 2nd, and 3rd thermal degradation steps of Ni^{2+} complex using CR method.

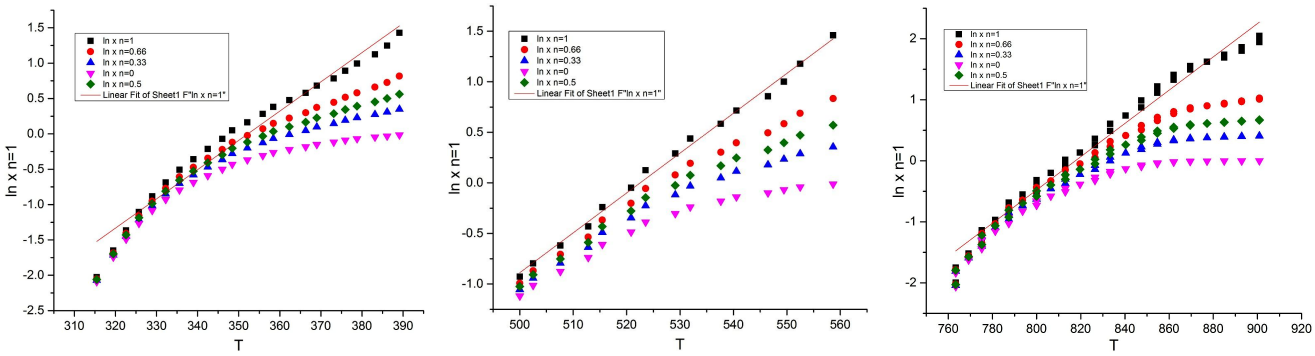

(a) (b) (c)

Figure 10: 1st, 2nd, and 3rd thermal degradation steps of Ni^{2+} complex using HM method.

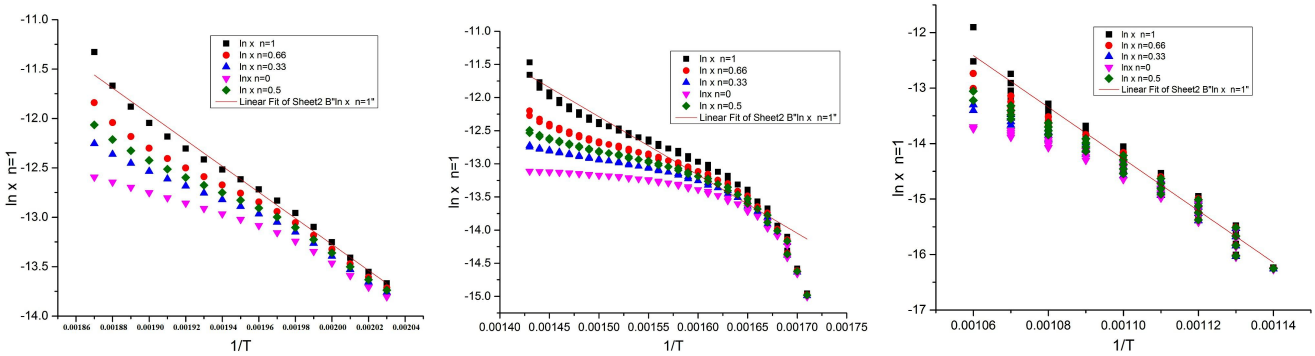

(a) (b) (c)

Figure 11: 1st, 2nd, and 3rd thermal degradation steps of Pt^{4+} complex using CR method.

decomposition steps for the complexes are tabulated in Table 3.

3.4. Results of kinetic data together with the thermal degradation steps of complexes

The results of kinetic data of the isolated complexes (Ni^{2+}, Pt^{4+}, and Cu^{2+}) as well as the thermodynamic parameters of activation were calculated by Eyring equation [43]. All the data are recorded in Table 4 by two isothermal methods such as Coats-Redfern (CR) [44] (Figures 9, 11, and 13) and Horowitz-Metzger (HM) [45] methods (Figures 10, 12, and 14).

The results in Table 4 pointed out to the following remarks:

(i) The stages of decomposition illustrate that the best fit is when $n = 1$, while the other values for n did not fit the best correlation.

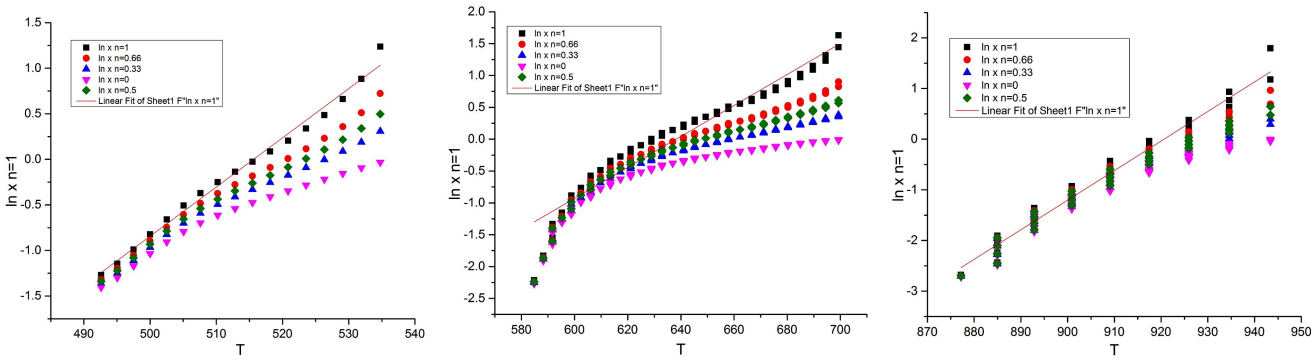

(a) (b) (c)

Figure 12: 1st, 2nd, and 3rd thermal degradation steps of Pt^{4+} complex using HM method.

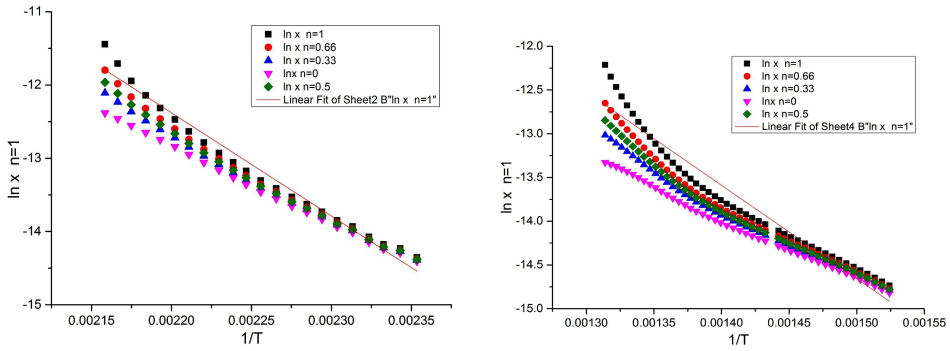

(a) (b)

Figure 13: 1st and 2nd thermal degradation steps of Cu^{2+} complex using CR method.

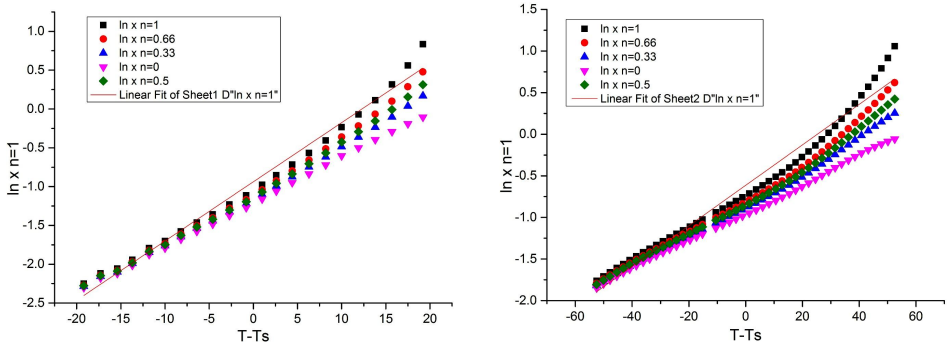

(a) (b)

Figure 14: 1st and 2nd thermal degradation steps of Cu^{2+} complex using HM method.

(ii) ΔG^* with positive values suggest that the decomposition steps are a nonspontaneous process since the free energy of the final residue is higher than the initial compound. ΔG^* values increase since the value of $T\Delta S^*$ are higher than the value of ΔH^* [46,47].

(iii) All the decomposition stages are an endothermic process since the values of ΔH^* have positive values.

(iv) ΔS^* of the decomposition steps have positive values suggesting that the disordered structure of the activated fragments is less than that of the undecomposed complex and consequently the decomposition reactions are slow [43].

3.5. Cyclic voltammetry (CV)

The redox properties of Cu^{2+} complex was studied by CV technique as shown in Figure 15. The measurements of Cu^{2+} complex (10^{-3} M) were officiated in a nonaqueous DMF solution containing the supporting electrolyte 0.1 M

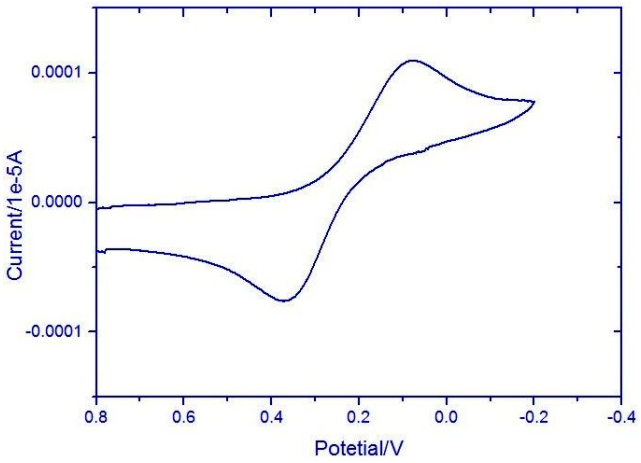

Figure 15: Cyclic-voltammetry of Cu(II) complex.

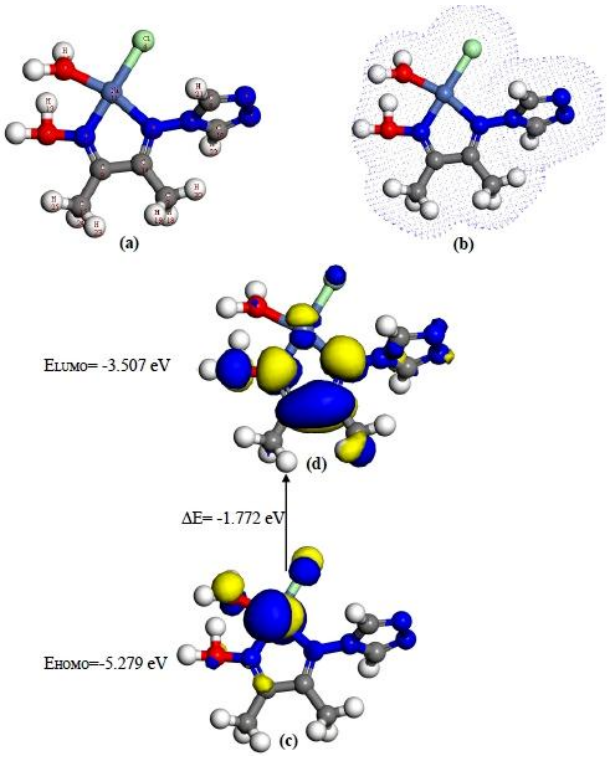

Figure 16: Molecular modeling of (a) Ni^{2+} complex, (b) electron density, (c) HOMO, and (d) LUMO.

of $[(n\text{-Bu})_4\text{N}]PF_6$ within the potential range from 0.8 V to -0.4 V at scan rate 100 mV/s. The Cu^{2+} complex exhibits quasi-reversible reduction waves at positive potentials for one electron transfer and at $E_{1/2} = 0.227$ V, $\Delta E = 286$ mV, where $E_{pc} = +0.084$ V and $E_{pa} = +0.37$ V (Cu^{2+}/Cu^{+}).

3.6. Molecular computational calculation using DFT

The structures of metal complexes together with the atom numbering are depicted in Figures 16–18. The following

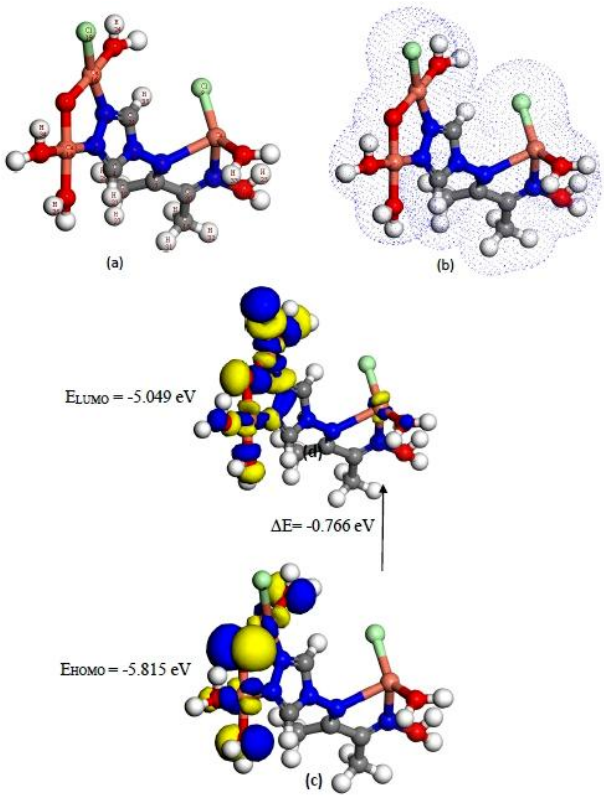

Figure 17: Molecular modeling of (a) Cu^{2+} complex, (b) electron density, (c) HOMO, and (d) LUMO.

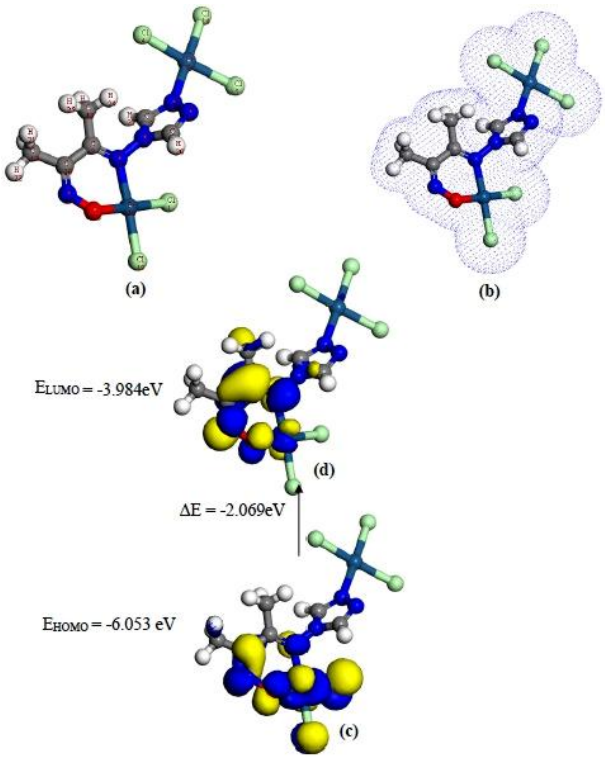

Figure 18: Molecular modeling of (a) Pt^{4+} complex, (b) electron density, (c) HOMO, and (d) LUMO.

Table 5: Calculated E_{HOMO}, E_{LUMO}, energy band gap (EH-EL), chemical potential (μ), electronegativity (χ), global hardness (η), global softness (S), and global electrophilicity index (ω) for the new complexes.

Compound	EH (eV)	EL (eV)	(EH-EL) (eV)	χ (eV)	μ (eV)	η (eV)	S (eV^{-1})	ω (eV)	σ (eV)
Ni^{2+} complex	−5.279	−3.507	−1.772	4.39	−4.39	0.886	0.443	10.87	1.12
Cu^{2+} complex	−5.815	−5.049	−0.766	5.43	−5.43	0.383	0.192	38.49	2.61
Pt^{4+} complex	−6.053	−3.984	−2.069	5.02	−5.02	1.035	0.517	12.17	0.966

Table 6: Some of energetic properties for the new complexes using DFT method.

Compound	HOMO (eV)	LUMO (eV)	Binding energy (Kcal/mol)	Kinetic energy (Kcal/mol)	Total energy (Kcal/mol)
Ni^{2+} complex	−5.279	−3.507	−2526.56	−3784.12	-8.23×10^5
Cu^{2+} complex	−5.815	−5.049	−3168.67	−11031.58	-16.0×10^5
Pt^{4+} complex	−6.053	−3.984	−2514.00	−7854.46	-20.54×10^5

remarks are obtained from the results of bond angles and lengths.

(i) The bond distance

N(6)−C(21), N(2)−C(7), N(2)−N(6), N(22)−C(21), N(6)−C(4), C(20)−N(1), and N(3)−C(4)

in the separated complex switched to be longer than that of L as a result of the formation of M−O and M−N bonds.

(ii) Upon coordination the bond angles of L are amended to some degree; such

N(2)−C(7)−C(20), N(2)−C(7)−C(12), C(20)−C(7)−C(12), C(21)−N(6)−N(2), C(21)−N(6)−C(4), and N(2)−N(6)−C(4)

angles are decreased or increased on bonding as a result of bonding.

(iii) The bond angles in Pt^{4+} and Cu^{2+} complexes afforded square-planar geometry, while Ni^{2+} complex shows tetrahedral geometry with sp^3 geometry. Finally, Cd^{2+} complex illustrates octahedral geometry.

(iv) We can predict an increase in the molecular weight and a decrease in the gas phase energy on the basis of the data in Table 5.

(v) The energy of both HOMO (π-donor) and LUMO (π-acceptor) is important in quantum chemical monographs, since the orbital behaves as an electron donor and known as a HOMO while the orbital acts as an electron acceptor and nominated as a LUMO. These molecular orbitals are known as frontier molecular orbitals (FMOs).

Table 5 depicted the chemical reactivity and site selectivity of the molecular systems by the DFT method concept. The energies of ($E_{HOMO}+E_{LUMO}$) and energy band gap ($E_{HOMO}-E_{LUMO}$) which feigned the end charge-transfer interaction within the molecule, electronegativity (χ), chemical potential (μ), global hardness (η), global softness (S) and global electrophilicity index (ω) are recorded in Table 5 [48,49,50]. The characterizations of kinetic stability and chemical reactivity of compounds depend on the energy gap ($E_{HOMO}-E_{LUMO}$) which is considered the main stability index that facilities the description. Upon the group that enters in the conjugation, the low value of energy gap suggests the easier of charge-transfer which influences the biological activity of the compounds. It is well known that the soft ligand with small gap is more reactive and more polarized than the hard one due to the ease in donating electron to the acceptor. Table 6 illustrates some of energies the isolated complexes.

3.7. Mass spectra

The mass spectrum of $[Cu_3LCl_2(H_2O)_5]4Cl$ (Figure 19) shows a peak at 660.91 [m/z] that coincides with the estimated value (660.61), which indicates that the formula of the compound is corrected. The fragmentation manner of the Cu^{2+} chelate (2:1) is depicted in Scheme 1. Also, the results of elemental analysis and thermal analyses are wielded to emphasize the suggested formula.

The mass spectrum of $[Pt_2LCl_5(H_2O)_{0.5}(EtOH)_{0.5}]3Cl$ (Figure 20) exposes the molecular ion peak at 874.24 [m/z], which is in agreement with the theoretical value (873.0). This proposes that the suggested formula of this compound is approved with the experimental data. Scheme 2 explored the fragments of the Pt(IV) complex (1:1). The data of elemental and thermal analysis are also taken as an evidence for that assumption. The mass spectrum indicates the dissociation of Pt(IV) complex.

3.8. Biological studies

3.8.1. Antitumor activity

The in vitro cytotoxicity of L and its complexes was scanted by MTT-based assays [35,36,51]. Through colorimetric technique, MTT assay is considered an adequate method to decide the cytotoxicity and for measuring cell growth. It is known that the yellow color of [MTT; 3-(4,5-dimethylthiazol-2-yl)-2,5-diphenyltetrazolium bromide]

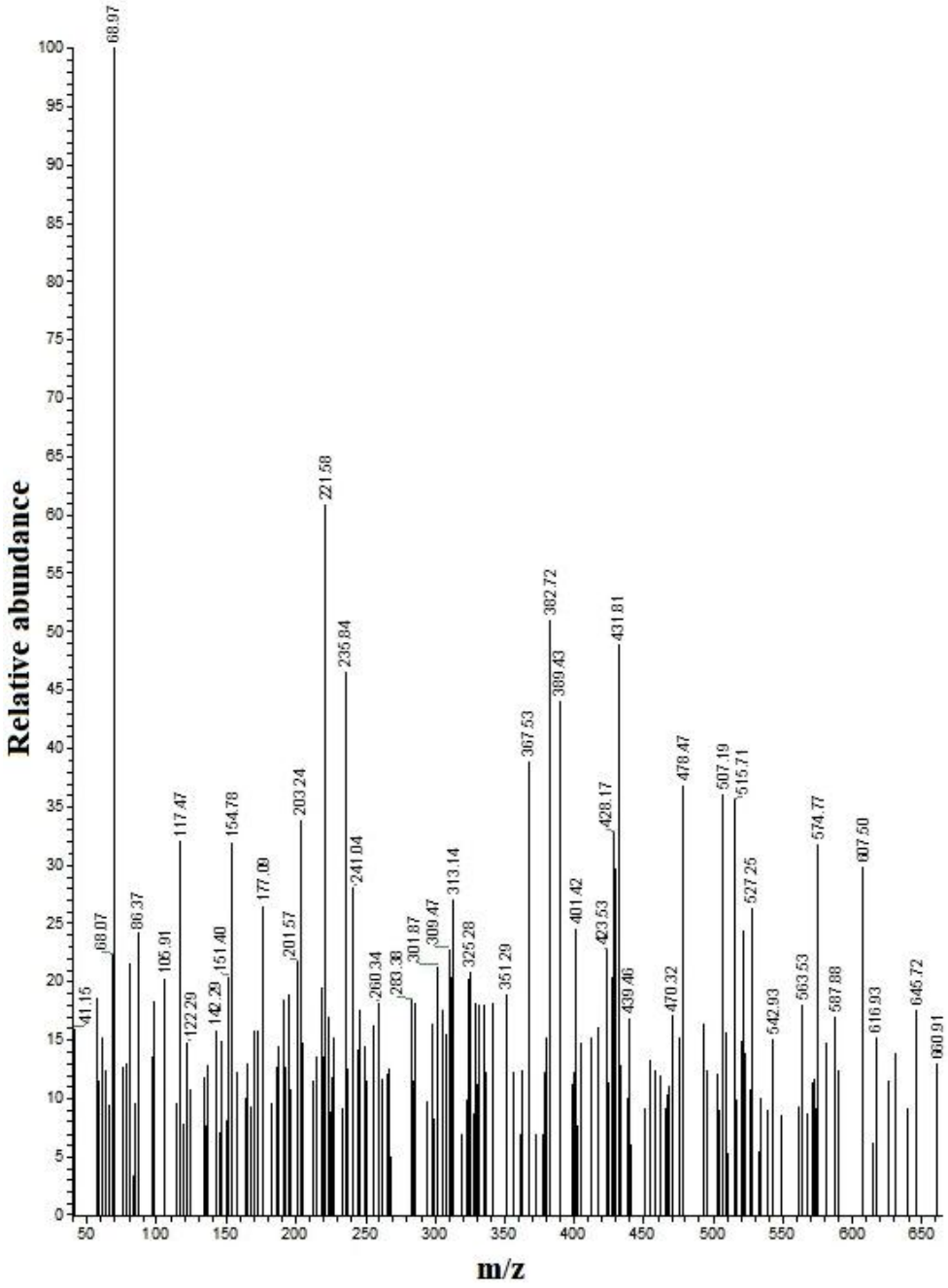

Figure 19: Mass spectra of $[Cu_3LCl_2(H_2O)_5]4Cl$.

changes to purple due to the formation of formazan via mitochondrial dehydrogenases of the cells [52]. The purple formazan which is insoluble becomes soluble on the addition of suitable solvent to form the colored solution. And hence the value of the absorbance at specific wavelength of the colored solution was purposed. In comparing the cured cells with the compounds and those obtained by unreacted control cells of the amount of purple formazan formed, we get the efficacy of the complexes in triggering death of cells concluded by the formation of a potion response curve and the results are shown in Table 7. The data obtained show that the estimating of L has availed chemotherapy since it exhibits a very strong activity towards mammary gland breast (MCF-7) and human cervical epithelioid carcinoma (Hela) with IC_{50} values of 7.91 μg/mL and 6.83 μg/mL, respectively. Also, the ligand has a strong activity against prostate cell line (PC-3) with IC_{50} value of 12.13 μg/mL. Almost the same result is with the Ni(II) complex as it has a very strong activity towards (MCF-7) and (Hela) with IC_{50} values of 9.98 μg/mL and

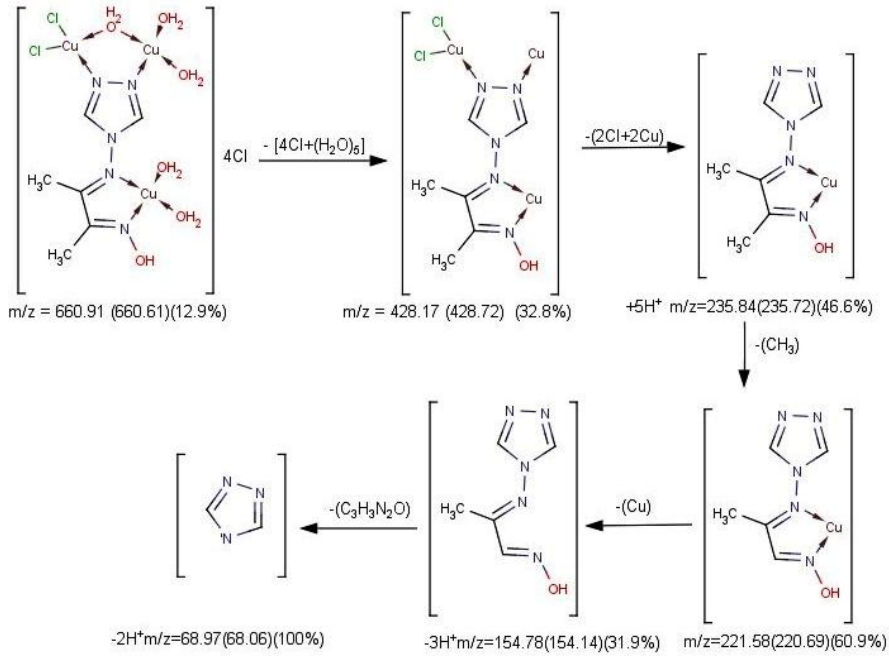

Scheme 1: The fragmentation manner of $[Cu_3LCl_2(H_2O)_5]4Cl$.

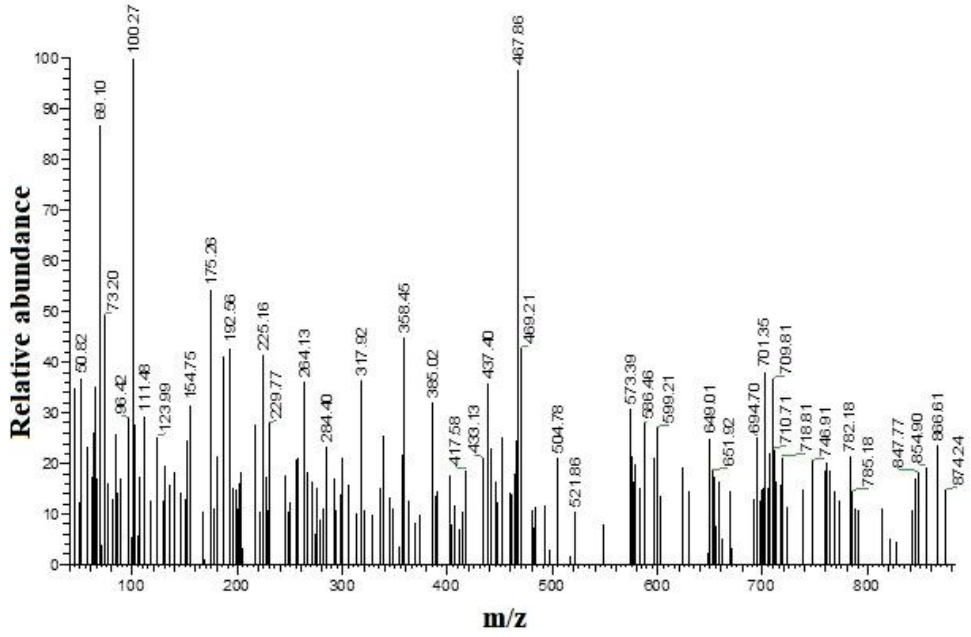

Figure 20: Mass spectra of $[Pt_2LCl_5(H_2O)_{0.5}(EtOH)_{0.5}]3Cl$.

8.14 μg/mL, while it exhibits a strong activism towards (PC-3) with IC_{50} values of 16.97 μg/mL. In addition to that the Cu(II) chelate has a strong IC_{50} value in (MCF-7) and (Hela) and a moderate activity against (PC-3) cell line. On the other hand, in (Hela) cell line, Cd^{2+} complex exhibits a moderate cytotoxicity effect, while the Pt^{4+} chelate has a weak IC_{50} in the same cancer cell line. The extent of the activities of ligand and its complexes lies between very strong and moderate to weak as shown in Figure 21.

3.8.2. DNA/methyl green colorimetric assay of the DNA-binding compounds

Green methyl dye reacts with DNA and produces a dyed DNA-methyl green in which the product of an addition reaction is reversible. This color remains unchanged in neutral pH, in which the free methyl green disappeared at this pH value. DNA-binding active compounds dislodge DNA from its methyl green complex. Upon alteration of DNA from methyl green by intercollators DNA, adding of

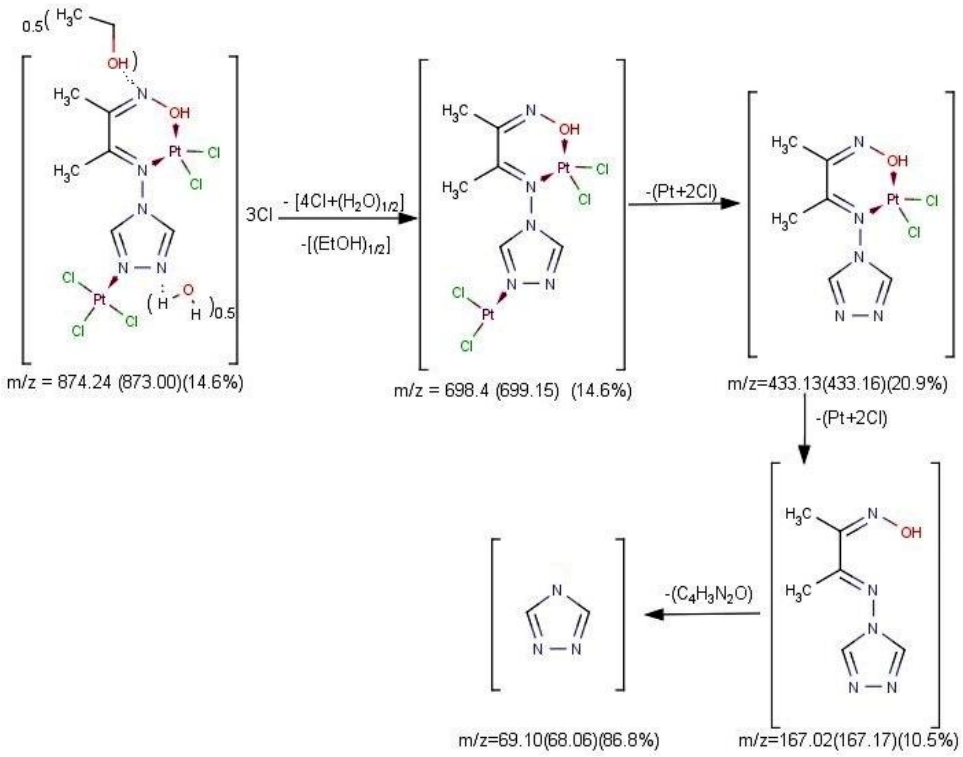

Scheme 2: The fragmentation manner of $[Pt_2LCl_5(H_2O)_{0.5}(EtOH)_{0.5}]3Cl$.

Table 7: Cytotoxic activity of the ligand and some metal complexes against human tumor cells.

No.	Compound	In vitro cytotoxicity IC_{50} (μM)*		
		MCF-7	PC3	Hela
	DOX**	4.17 ± 0.2	8.87 ± 0.6	5.57 ± 0.4
1	L	7.91 ± 0.5	12.13 ± 1.0	6.83 ± 0.5
2	Pt^{4+}	53.26 ± 3.3	67.52 ± 3.9	62.40 ± 3.7
3	Cu^{2+}	14.16 ± 1.2	26.91 ± 1.7	15.27 ± 1.4
4	Cd^{2+}	18.02 ± 1.4	35.26 ± 2.5	22.36 ± 1.8
5	Ni^{2+}	9.98 ± 0.8	16.97 ± 1.3	8.14 ± 0.7

*IC_{50} (μM): 1–10 (very strong). 11–20 (strong). 21–50 (moderate). 51–100 (weak) and above 100 (noncytotoxic).
**DOX: Doxorubicin.

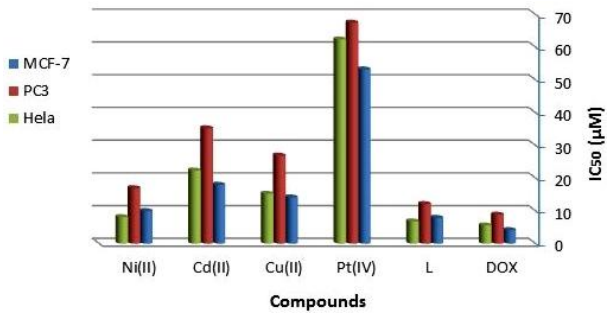

Figure 21: Cytotoxic activity of some compounds against human tumor cells.

water to the dye was allowed, which led to the development of the pale carbinol, then the absorbance declines as observed from the colorimetric curves. The offset was calculated by a spectrophotometric assay as a decrease in the absorbance at 630 nm. The results were announced as inhibition concentration 50% value (IC_{50}) calculated by linear regression of data plotted on a semi-log scale and represented in Table 8. In this assay, doxorubicin was used as a control. Doxorubicin or Adriamycin, this drug belongs to a group of antitumor medications or the so-called antimetabolic drugs. It works to stop the growth of tumor cells by interfering with the DNA, which is the genetic material present in the cell. L displayed a very strong inhibitory activity and powerfully intercalate DNA at a decreased IC_{50} value in the range of $29.18 \pm 1.6\,\mu$M. Approximately, the activity of tested chelates is arranged in the order Ni(II) > Cu(II) > Cd(II) > Pt(IV) comparing to Doxorubicin with IC_{50} values as shown in Table 8.

3.8.3. Antioxidant activities

The ligand (L) and its metal complexes were examined for their antioxidant activity by the erythrocyte hemolysis. The results of the antioxidant activity with vitamin C are depicted in Table 9 and represented in Figure 22. The ligand showed a high antioxidant activity with respect to erythrocyte hemolysis. The activity of the tested complexes is arranged in the order Co(II) > Pd(II) > Fe(III) in comparison to vitamin C with respect to erythrocyte hemolysis.

Table 8: DNA/methyl green colorimetric assay of the DNA-binding compounds.

DNA-active compound	DNA/methyl green (IC_{50}, μg/mL)
DOX	31.27 ± 1.8
L	29.18 ± 1.6
Pt(IV)	82.27 ± 2.7
Cu(II)	38.02 ± 1.9
Cd(II)	45.35 ± 2.1
Ni(II)	34.71 ± 1.8

IC_{50} values represent the concentration (mean $\pm$ SD, $n = 3$–5 separate determinations) required for a 50% decrease in the initial absorbance of the DNA/methyl green solution.

Table 9: Antioxidant erythrocyte hemolysis assay for the ligand and isolated complexes.

No.	Compounds	Erythrocyte hemolysis (A/B $\times$ 100)	
		Absorbance of samples (A)	% Hemolysis
Absorbance of H_2O (B)		0.875	—
Vitamin C		0.030	3.4%
1	L	0.056	6.4%
2	Pt^{4+}	0.078	8.9%
3	Cu^{2+}	0.369	42.2%
4	Cd^{2+}	0.105	12.0%
5	Ni^{2+}	0.089	10.2%

3.8.4. Antibacterial and antifungal activity

In the antimicrobial activities, the ampicillin (a broad-field antibiotic) acts as a positive control for the antibacterial test while DMSO was utilized as a negative control and solvent. The diameter of inhibition zone of ampicillin towards *E. coli* is 25 mm and towards *S. aurous* is 21 mm. Table 10 depicts the results of the antibacterial test of the tested complexes towards Gram-negative (*E. coli*) and Gram-positive (*S. aurous*) bacterial strains. The Cd(II) complex shows the maximum antibacterial activity towards *E. coli* with 24 mm inhibition zone diameter. On the other hand, the complexes of Cu(II) and Ni(II) manifested a sensible antibacterial activity towards *E. coli* with 13 mm and 12 mm inhibition zone diameter, respectively. Pt(IV) complex exhibits the weakest antibacterial activity recording 5 mm inhibition zone diameter. The antibacterial behavior of the examined chelates against Gram-positive bacterial strain *S. aureus* is illustrated in Table 10. The Cd(II) complex (31 mm) $>$ the reference antimicrobial ampicillin (21 mm) $>$ Pt(IV) (16 mm) $>$ Cu(II) (13 mm) $=$ Ni(II) (13 mm).

Amphotericin B (antifungal agent) recorded the antifungal activities towards the fungal strains *A. flavus* and *C. albicans* of 17 mm and 21 mm, respectively. Only Cd(II) and Cu(II) compounds exhibit an antifungal effectiveness towards fungal strain *C. albicans* with 27 mm and 11 mm inhibition zone diameter, respectively. While Ni(II) and Pt(IV) chelates do not display any antifungal reactivity

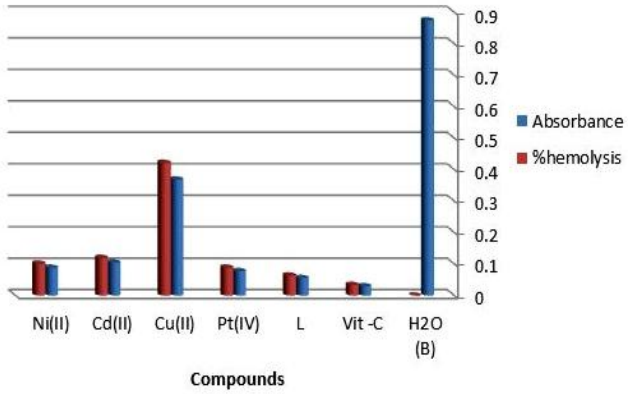

Figure 22: Antioxidant activity through erythrocyte hemolysis.

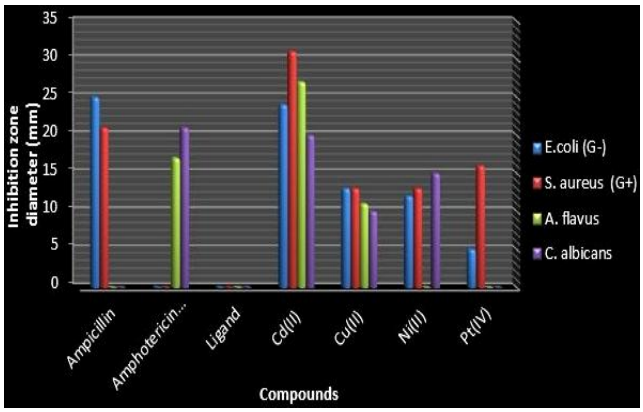

Figure 23: Antibacterial and antifungal activities of L and its complexes.

towards fungal strain *C. albicans*. Cd(II) complex shows a potent activity against fungal strain *A. flavus* and Ni(II) and Cu(II) compounds show moderate antifungal activities against fungal strain *A. flavus.* While Pt(II) complex does not show any antifungal activities against fungal strain *A. flavus*. It was perceived that the ligand has no effect against bacteria or fungi as represented in Table 10. The antimicrobial activities of L and its chelates are shown in Figure 23. The efficient and effective propagation of compounds via cell membrane or interaction with micro-organism cell wall give rise to a high antibacterial activity, which is known as lipophilic characteristics (i.e., penetrating the lipid cell wall linked to the polarity of central metal ion and raised with the formation of chelation ring, sharing the positive charge on metal ion with the N-donor atom of L causing π-electron delocalization on the chelation ring, which is also corroborated by the works in [53,54,55]).

$$\%\text{Activity index} = \frac{\text{Zone of inhibition by test compound (diameter)}}{\text{Zone of inhibition by standard (diameter)}} \times 100.$$

Table 10: Antimicrobial activity of the isolated compounds.

Sample		Inhibition zone diameter (mm/mg sample)							
		Bacteria				Fungi			
		E. coli (G^-)	% A.I.	*S. aureus* (G^+)	% A.I.	*A. flavus*	% A.I.	*C. albicans*	% A.I.
Standard	Ampicillin: antibacterial agent	25	100	21	100	—	—	—	—
	Amphotericin B: antifungal agent	—	—	—	—	17	100	21	100
Control; DMSO		0.0	0.0	0.0	0.0	0.0	0.0	0.0	0.0
Ligand		0.0	0.0	0.0	0.0	0.0	0.0	0.0	0.0
Cd(II) complex		24	96	31	147	27	158	20	95
Cu(II) complex		13	52	13	62	11	64	10	48
Ni(II) complex		12	48	13	62	0.0	0.0	15	71
Pt(IV) complex		5	20	16	76	0.0	0.0	0.0	0.0

% A.I.: % Activity index.

4. Conclusions

A novel ligand, 3-(3H-1,2,4-triazole-4-(5H)-ylimino)butane-2-one-oxime (L), and its complexes were synthesized and characterized using chemical, spectral (FTIR, UV-Vis, mass), cyclic voltammetry, and magnetic measurements. Electronic spectra and magnetic measurements of the complexes suggest a structure that is tetrahedral for Ni^{2+}, octahedral for Cd^{2+}, while square-planar for Cu^{2+} and Pt^{4+} complexes. Also, DFT parameters were applied for Cu^{2+}, Ni^{2+}, and Pt^{4+} complexes which prove the geometry of L towards the metal ions. Kinetic and thermodynamic parameters of the isolated complexes were calculated by CR and HM methods. The biological activity of L and its complexes was tested against three types of cancer cell lines, and against different bacterial strains.

Acknowledgments This article is based on a M.Sc. thesis entitled "Spectroscopic, cyclic voltammetry and biological studies of some complexes derived from dialkyl hydrazines and oximes of some metal ions" by Doaa E. El-Kholy in "2020" at "Mansoura University, Egypt".

Conflict of interest The authors declare that they have no conflict of interest.

References

[1] G. Aromí, L. A. Barrios, O. Roubeau, and P. Gamez, *Triazoles and tetrazoles: Prime ligands to generate remarkable coordination materials*, Coord Chem Rev, 255 (2011), 485–546.

[2] C.-H. Zhou and Y. Wang, *Recent researches in triazole compounds as medicinal drugs*, Curr Med Chem, 19 (2012), 239–280.

[3] J. G. Haasnoot, *Mononuclear, oligonuclear and polynuclear metal coordination compounds with 1,2,4-triazole derivatives as ligands*, Coord Chem Rev, 200-202 (2000), 131–185.

[4] N. A. Al-Masoudi, Y. A. Al-Soud, and W. A. Al-Masoudi, *Thiosugar nucleosides. Synthesis and biological activity of 1,3,4-thiadiazole, thiazoline and thiourea derivatives of 5-thio-D-glucose*, Nucleosides Nucleotides Nucleic Acids, 23 (2004), 1739–1749.

[5] Y. Naito, F. Akahoshi, S. Takeda, T. Okada, M. Kajii, H. Nishimura, et al., *Synthesis and pharmacological activity of triazole derivatives inhibiting eosinophilia*, J Med Chem, 39 (1996), 3019–3029.

[6] E. De Clercq, *Antiviral drugs in current clinical use*, J Clin Virol, 30 (2004), 115–133.

[7] X. Collin, A. Sauleau, and J. Coulon, *1,2,4-Triazolo mercapto and aminonitriles as potent antifungal agents*, Bioorg Med Chem Lett, 13 (2003), 2601–2605.

[8] Z. Sui, J. Guan, D. J. Hlasta, M. J. Macielag, B. D. Foleno, R. M. Goldschmidt, et al., *SAR studies of diaryltriazoles against bacterial two-component regulatory systems and their antibacterial activities*, Bioorg Med Chem Lett, 8 (1998), 1929–1934.

[9] J. B. Hester Jr, A. D. Rudzik, and B. V. Kamdar, *6-phenyl-4H-s-triazolo[4,3-a][1,4]benzodiazepines which have central nervous system depressant activity*, J Med Chem, 14 (1971), 1078–1081.

[10] N. A. Al-Masoudi, Y. A. Al-Soud, and I. A. I. Ali, *Synthesis of 1,2,4-triazole C-nucleosides from hydrazonyl chlorides and nitriles*, Nucleosides Nucleotides Nucleic Acids, 26 (2007), 37–43.

[11] K. M. Khan, S. Siddiqui, M. Saleem, M. Taha, S. M. Saad, S. Perveen, et al., *Synthesis of triazole Schiff bases: Novel inhibitors of nucleotide pyrophosphatase/phosphodiesterase-1*, Bioorg Med Chem, 22 (2014), 6509–6514.

[12] P. A. Lambert, K. D. Somers, E. C. Kohn, and R. R. Perry, *Antiproliferative and antiinvasive effects of carboxyamidotriazole on breast cancer cell lines*, Surgery, 122 (1997), 372–379.

[13] H. T. Akçay and R. Bayrak, *Computational studies on the anastrozole and letrozole, effective chemotherapy drugs against breast cancer*, Spectrochim Acta A Mol Biomol Spectrosc, 122 (2014), 142–152.

[14] M. Clemons, R. E. Coleman, and S. Verma, *Aromatase inhibitors in the adjuvant setting: bringing the gold to a standard?*, Cancer Treat Rev, 30 (2004), 325–332.

[15] O. Bekircan and H. Bektas, *Synthesis of new bis-1,2,4-triazole derivatives*, Molecules, 11 (2006), 469–477.

[16] J. M. Kane, B. M. Baron, M. W. Dudley, S. M. Sorensen, M. A. Staeger, and F. P. Miller, *2,4-Dihydro-3H-1,2,4-triazol-3-ones as anticonvulsant agents*, J Med Chem, 33 (1990), 2772–2777.

[17] I. Küçükgüzel, S. G. Küçükgüzel, S. Rollas, G. Otük-Sanis, O. Ozdemir, I. Bayrak, et al., *Synthesis of some 3-(arylalkylthio)-4-alkyl/aryl-5-(4-aminophenyl)-4H-1,2,4-triazole derivatives and their anticonvulsant activity*, Farmaco, 59 (2004), 893–901.

[18] B. E. Gilbert and V. Knight, *Biochemistry and clinical applications of ribavirin*, Antimicrob Agents Chemother, 30 (1986), 201–205.

[19] B. Shivarama Holla, B. Veerendra, M. K. Shivananda, and B. Poojary, *Synthesis characterization and anticancer activity studies on some Mannich bases derived from 1,2,4-triazoles*, Eur J Med Chem, 38 (2003), 759–767.

[20] G. Turan-Zitouni, M. Sivaci, F. S. Kiliç, and K. Erol, *Synthesis of some triazolyl-antipyrine derivatives and investigation of analgesic activity*, Eur J Med Chem, 36 (2001), 685–689.

[21] O. Bekircan, M. Küxük, B. Kahveci, and S. Kolayli, *Convenient synthesis of fused heterocyclic 1,3,5-triazines from some N-acyl imidates and heterocyclic amines as anticancer and antioxidant agents*, Arch Pharm (Weinheim), 338 (2005), 365–372.

[22] P. C. Wade, B. R. Vogt, T. P. Kissick, L. M. Simpkins, D. M. Palmer, and R. C. Millonig, *1-Acyltriazoles as antiinflammatory agents*, J Med Chem, 25 (1982), 331–333.

[23] A. K. Gupta and K. P. Bhargava, *Some triazole analogs as anti-inflammatory agents*, Pharmazie, 33 (1978), 430–431.

[24] B. Modzelewska-Banachiewicz and J. Kalabun, *Synthesis and biological action of 5-oxo-1,2,4-triazine derivatives*, Pharmazie, 54 (1999), 503–505.

[25] Y. A. Al-Soud, M. N. Al-Dweri, and N. A. Al-Masoudi, *Synthesis, antitumor and antiviral properties of some 1,2,4-triazole derivatives*, Farmaco, 59 (2004), 775–783.

[26] A. A. Siddiqui, R. Mishra, M. Shaharyar, A. Husain, M. Rashid, and P. Pal, *Triazole incorporated pyridazinones as a new class of antihypertensive agents: design, synthesis and in vivo screening*, Bioorg Med Chem Lett, 21 (2011), 1023–1026.

[27] G. H. Jeffery, J. Bassett, J. Mendham, and R. C. Denney, *Vogel's Textbook of Quantitative Chemical Analysis*, Longman Scientific and Technical, Essex, England, 5th ed., 1989.

[28] D. E. El-Kholy, A. H. El-Askalany, and M. M. Mostafa, *Single crystal X-ray of 1-[(1,2,4-triazole-4yl)imino]diacetyl monoxime (L) as a novel triazole and the characterization and biological studies of its chelates of Co^{2+}, Pd^{2+} and Fe^{3+}*, Appl Organomet Chem (to appear).

[29] A. Altomare, G. Cascarano, C. Giacovazzo, A. Guagliardi, M. Burla, G. Polidori, et al., *SIR92 – a program for automatic solution of crystal structures by direct methods*, J Appl Crystallogr, 27 (1994), 435–436.

[30] B. Delley, *An all-electron numerical method for solving the local density functional for polyatomic molecules*, J Chem Phys, 92 (1990), 508.

[31] B. Delley, *A scattering theoretic approach to scalar relativistic corrections on bonding*, Int J Quantum Chem, 69 (1998), 423–433.

[32] B. Delley, *From molecules to solids with the $DMol^3$ approach*, J Chem Phys, 113 (2000), 7756.

[33] X. Wu and A. Ray, *Density-functional study of water adsorption on the PuO_2(110) surface*, Phys Rev B, 65 (2002), 085403.

[34] A. Kessi and B. Delley, *Density functional crystal vs. cluster models as applied to zeolites*, Int J Quantum Chem, 68 (1998), 135–144.

[35] F. Denizot and R. Lang, *Rapid colorimetric assay for cell growth and survival. modifications to the tetrazolium dye procedure giving improved sensitivity and reliability*, J Immunol Methods, 89 (1986), 271–277.

[36] M. I. Thabrew, R. D. Hughes, and I. G. McFarlane, *Screening of hepatoprotective plant components using a HepG2 cell cytotoxicity assay*, J Pharm Pharmacol, 49 (1997), 1132–1135.

[37] P. Piliouras, G. C. Ulett, C. Ashhurst-Smith, R. G. Hirst, and R. E. Norton, *A comparison of antibiotic susceptibility testing methods for cotrimoxazole with Burkholderia pseudomallei*, Int J Antimicrob Agents, 19 (2002), 427–429.

[38] M. A. Pfaller, L. Burmeister, M. S. Bartlett, and M. G. Rinaldi, *Multicenter evaluation of four methods of yeast inoculum preparation*, J Clin Microbiol, 26 (1988), 1437–1441.

[39] Y. Morimoto, K. Tanaka, Y. Iwakiri, S. Tokuhiro, S. Fukushima, and Y. Takeuchi, *Protective effects of some neutral amino acids against hypotonic hemolysis*, Biol Pharm Bull, 18 (1995), 1417–1422.

[40] S. H. Etaiw, T. A. Fayed, M. M. El-bendary, and H. Marie, *Three-dimensional coordination polymers based on trimethyltin cation with nicotinic and isonicotinic acids as anticancer agents*, Appl Organomet Chem, 32 (2018), e4066.

[41] K. Nakamoto, *Infrared and Raman Spectra of Inorganic and Coordination Compounds, Part A: Theory and Applications in Inorganic Chemistry*, John Wiley & Sons, New York, 6th ed., 2009.

[42] A. B. P. Lever, *Inorganic Electronic Spectroscopy*, Elsevier, Amsterdam, 1968.

[43] A. A. Frost and R. G. Pearson, *Kinetics and Mechanism*, John Wiley & Sons, New York, 2nd ed., 1961.

[44] A. Coats and J. Redfern, *Kinetic parameters from thermogravimetric data*, Nature, 201 (1964), 68–69.

[45] H. H. Horowitz and G. Metzger, *A new analysis of thermogravimetric traces*, Anal Chem, 35 (1963), 1464–1468.

[46] P. B. Maravalli and T. R. Goudar, *Thermal and spectral studies of 3-N-methyl-morpholino-4-amino-5-mercapto-1,2,4-triazole and 3-N-methyl-piperidino-4-amino-5-mercapto-1,2,4-triazole complexes of cobalt(II), nickel(II) and copper(II)*, Thermochim Acta, 325 (1999), 35–41.

[47] R. Sreekala and K. K. M. Yusuff, *Thermal decomposition kinetics of iron(III), cobalt(II), nickel(II) and copper(II) complexes of a Schiff base derived from quinoxaline-2-carboxaldehyde and glycine*, React Kinet Catal Lett, 48 (1992), 575–581.

[48] R. G. Pearson, *Absolute electronegativity and hardness: applications to organic chemistry*, J Org Chem, 54 (1989), 1423–1430.

[49] J. Padmanabhan, R. Parthasarathi, V. Subramanian, and P. K. Chattaraj, *Electrophilicity-based charge transfer descriptor*, J Phys Chem A, 111 (2007), 1358–1361.

[50] R. Parthasarathi, J. Padmanabhan, U. Sarkar, B. Maiti, V. Subramanian, and P. K. Chattaraj, *Toxicity analysis of benzidine through chemical reactivity and selectivity profiles: A DFT approach*, Internet Electron J Mol Des, 2 (2003), 798–813.

[51] T. Mosmann, *Rapid colorimetric assay for cellular growth and survival: application to proliferation and cytotoxicity assays*, J Immunol Methods, 65 (1983), 55–63.

[52] I. Isobe, K. Yanagisawa, and M. Michikawa, *3-(4,5-Dimethylthiazol-2-yl)-2,5-diphenyltetrazolium bromide (MTT) causes Akt phosphorylation and morphological changes in intracellular organellae in cultured rat astrocytes*, J Neurochem, 77 (2001), 274–280.

[53] Z. H. Chohan, *Synthesis and biological properties of Cu(II) complexes with 1,1′-disubstituted ferrocenes*, Synth React Inorg Met Org Chem, 34 (2004), 833–846.

[54] Z. H. Chohan, C. T. Supuran, and A. Scozzafava, *Metalloantibiotics: synthesis and antibacterial activity of cobalt(II), copper(II), nickel(II) and zinc(II) complexes of kefzol*, J Enzyme Inhib Med Chem, 19 (2004), 79–84.

[55] Z. H. Chohan, M. Arif, M. A. Akhtar, and C. T. Supuran, *Metal-based antibacterial and antifungal agents: synthesis, characterization, and in vitro biological evaluation of Co(II), Cu(II), Ni(II), and Zn(II) complexes with amino acid-derived compounds*, Bioinorg Chem Appl, 2006 (2006), 83131.